ACS APPLIED MATERIALS & INTERFACES

www.acsami.org

Research Article

A Transferrable, Adaptable, Free-Standing, and Water-Resistant Hyperbolic Metamaterial

Hung-I Lin, Hsiang-Yao Tan, Yu-Ming Liao, Kun-Ching Shen, Mikhail Y. Shalaginov, Monika Kataria, Chih-Ting Chen, Jun-Wei Chang, and Yang-Fang Chen*

Cite This: *ACS Appl. Mater. Interfaces* 2021, 13, 49224–49231

Read Online

ACCESS | Metrics & More | Article Recommendations | Supporting Information

ABSTRACT: Hyperbolic metamaterials (HMMs) have attracted significant attention due to the profound manipulation of the photonic density of states, resulting in the efficient optoelectronic devices with the enhanced light−matter interaction. HMMs are conventionally built on rigid large-size substrates with poor conformability and the absence of flexibility. Here, we demonstrate a grating collageable HMM (GCHMM), which is composed of eight alternating layers of Au and poly(methyl methacrylate) (PMMA) and PMMA grating nanostructure containing quantum dots (QDs). The QDs serve as a scattering gain medium performing a random laser action, and the grating nanostructure enhances the extraction of light from QDs. The GCHMM enhances laser action by 13 times, reduces lasing threshold by 46%, and increases differential quantum efficiency by 1.8 times as compared to a planar collageable HMM. In addition, the GCHMM can be retransferred multiple times to other substrates as well as provide sufficient protection in water and still retain an excellent performance. It also shows stable functionality even when transferred to a dental floss. The GCHMM, therefore, promises to become a versatile platform for foldable, adaptable, free-standing, and water-resistant optoelectronic device applications.

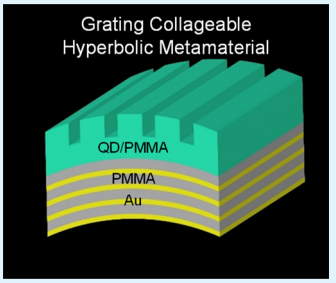

KEYWORDS: *hyperbolic metamaterial, optoelectronics, laser action, quantum dot, foldable*

INTRODUCTION

Recently, optoelectronic devices have been extensively adapted for technology advances in Internet of Things applications, including smart clothing, electronic skins, and artificial intelligent systems.[1−5] In order to successfully integrate optoelectronic devices on freeform surfaces for a variety of functionalities, these devices are required to feature high sensitivity, low energy consumption, long-term use, and sustainability under certain mechanical strain and bending conditions.[1,2] Flexible, rollable, stretchable, conformable, miniaturized, and user-friendly systems are needed to implement human-machine building blocks, such as flexible photodetectors, flexible optoelectronic fibers and textiles, stretchable laser systems, rollable metamaterial devices, etc.[6−12]

Hyperbolic metamaterials (HMMs), an emerging platform for enabling optoelectronic devices applications, have drawn significant attention owing to their profound manipulation of the photonic density of states (PDOS), which can increase the efficiency of optoelectronic devices.[13−15] In general, the HMMs are composed of alternating layers of metal-dielectric stacks, well-aligned metallic nanowires embedded in a dielectric medium, and core-multi-shell nanostructures.[13,16−18] The HMMs have been demonstrated to greatly enhance spontaneous and stimulated emission with reduced threshold, achieve a white lasing spectrum, increase charge-transfer dynamics, and serve as a platform for molecular bio-sensing with ultrahigh sensitivity.[19−25] To form a cavity with an ultrahigh effective index and achieve efficient light extraction, nano-patterned HMM structures are required.[26,27] However, such HMMs, typically built on top of rigid, non-flexible, bulky substrates, are unsuitable for mechanically flexible, foldable, and adaptable photonic meta-devices. Therefore, to meet the vast demands of optoelectronic device applications, there are still several obstacles that are needed to be overcome. Recently, HMMs have been proven to enhance random laser action.[17,21,28] A random laser is a unique physical system, where the light travels inside an optical gain medium following the closed loop paths formed by the multiple scattering processes as the feedback mechanism.[29−32] Due to optical cavity-free architectures, broad angular emission patterns, and white light pumping, random lasers have been considered as the new branch of next-generation light sources.[31,33−35] Interesting random-laser-based applications have been successfully demonstrated, such as highly flexible, stretchable, wearable, dissolvable, and self-healable optoelectronic devices.[7,36−39]

Received: August 13, 2021
Accepted: September 24, 2021
Published: October 5, 2021

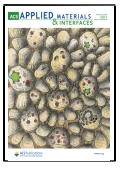

https://doi.org/10.1021/acsami.1c15481
ACS Appl. Mater. Interfaces 2021, 13, 49224–49231

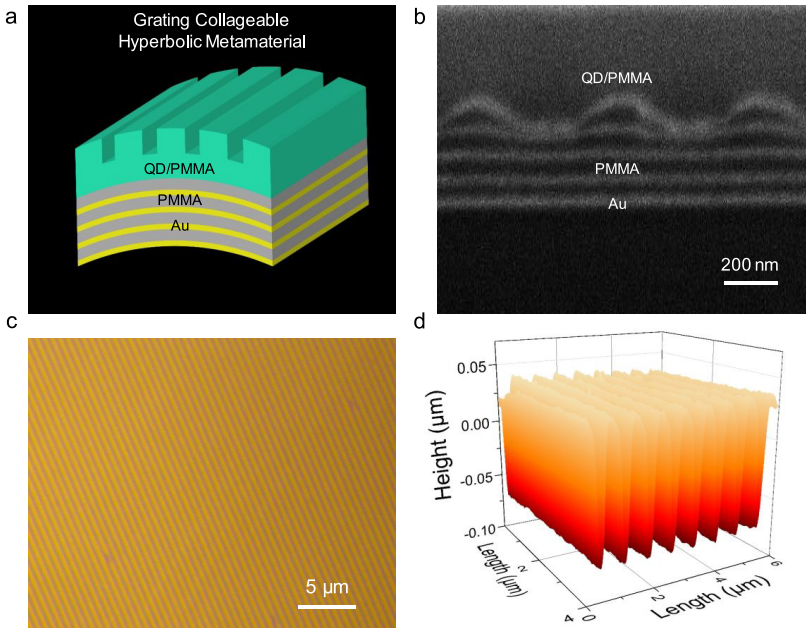

Figure 1. Grating collageable hyperbolic metamaterial (GCHMM). (a) Schematic diagram of GCHMM. (b) SEM image depicting a cross section of the free-standing GCHMM. The HMM is composed of eight alternating flexible layers of Au and PMMA with the respective thicknesses of 12 and 30 nm each. The CdSe/ZnS core-shell quantum dots (QDs) are embedded inside the top PMMA layer patterned as a periodical nanostructure. The period, width, and height of the grating nanostructure are 700, 300, and 100 nm, respectively. Morphologies of GCHMM under (c) optical and (d) atomic force microscopes.

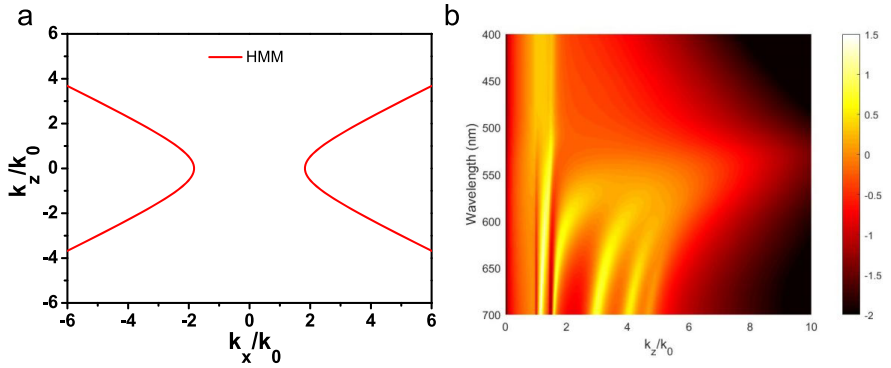

Figure 2. Theoretical analysis of HMM. (a) Iso-frequency curves of HMM considering the epsilons at the emission wavelength center for CdSe/ZnS QDs at 630 nm. (b) Normalized dissipated power spectrum considering the lossy Au components of HMM at a dipole distance away from the HMM of 5 nm. The spectrum is plotted in a logarithmic scale.

Here, we present a grating collageable HMM (GCHMM). The GCHMM contains four bi-layers of Au and poly(methyl methacrylate) (PMMA) without any support from the bottom substrate. By selecting the proper thicknesses and material components of the layers, the GCHMM is able to achieve an extremely anisotropic effective permittivity that boosts light–matter interactions. On top of the GCHMM, we defined a periodically PMMA grating nanostructure with embedded CdSe/ZnS core-shell type quantum dots (QDs). The QDs can serve as the multiple scattering gain medium for random laser action. These periodical nanostructures act as efficient light extractors. The whole GCHMM structure is mechanically foldable, conformable to freeform surfaces, and submicron-thick. As compared to the planar collageable HMM (PCHMM), which is the device without grating nanostructures, the GCHMM enables 13-fold enhancement of random-laser intensity, reduces the lasing threshold by 46%, and leads to 1.8-fold increase in differential quantum efficiency.[40] Additionally, the GCHMM is retransferable to other substrates as well as provides sufficient protection in water and still retains excellent performance. This stability makes GCHMM devices suitable for real wearable application, such as under certain force of deformation and being exposed to high humidity and even water. Interestingly, the realization of GCHMM includes several developments that, when combined together, offer unprecedented functionalities. First, the grating nanostructure is capable of accommodating several kinds of QDs that can interact with the tunable hyperbolic-metamaterial modes in a desirable spectral regime. Additionally, the GCHMM is a promising platform for realization of wearable skin sensors; it is also compatible with rollable color filters and displays. Therefore, the GCHMM is a unique building block for unlocking transferrable, adaptable, and free-standing optoelectronic devices.

https://doi.org/10.1021/acsami.1c15481
ACS Appl. Mater. Interfaces 2021, 13, 49224–49231

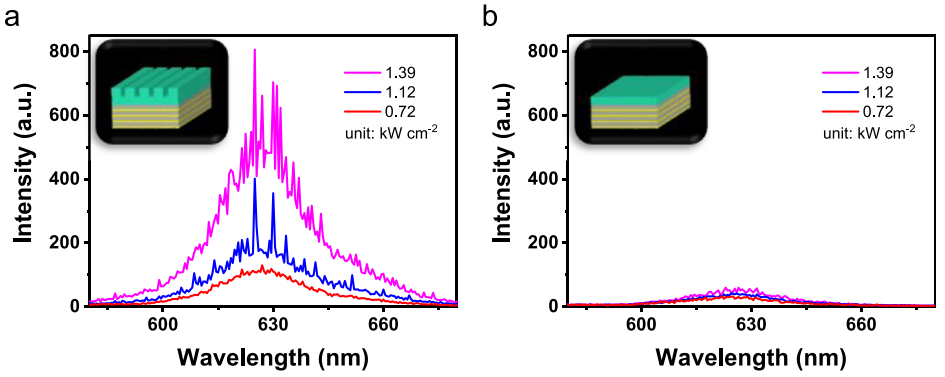

Figure 3. Emission spectra of random laser action. Panels (a) and (b) are the emission spectra of CdSe/ZnS QDs embedded inside the nanostructure layer and on top of the planar HMM for the GCHMM and PCHMM on Si substrates, respectively. The insets are the corresponding schemes. Three kinds of pumping energy densities are used to discover the random laser action. For the GCHMM, under a pumping energy density of 0.72 kW cm^{-2}, a typical spontaneous emission is observed. With further increasing the pumping energy densities to 1.12 and 1.39 kW cm^{-2}, random laser action with clearly sharp peaks emerge. For the PCHMM, under these three kinds of pumping energy densities, the spectra are spontaneous emissions. All the emission spectra were excited using a pulsed diode laser with a central wavelength of 374 nm at room temperature.

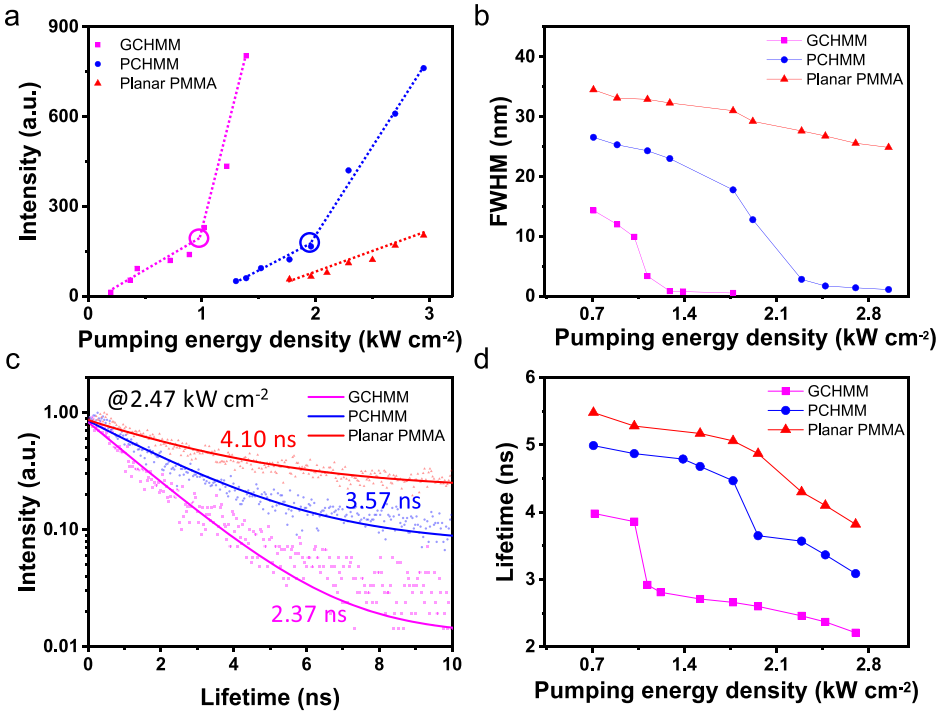

Figure 4. Characterizations of random laser action. (a) Maximum emission intensities plotted as a function of pumping energy intensities. The fitted lines with relatively flat slopes are spontaneous emissions, and those with relatively sharp slopes are stimulated emissions. The intersections (marked as hollow circles) between the flat and sharp slopes are the corresponding laser thresholds. The thresholds for the GCHMM and PCHMM are 1.05 and 1.95 kW cm^{-2}, respectively. (b) FWHM of the peak as a function of pumping energy intensities from (a). (c) Lifetime measurements under a pumping energy density of 2.47 kW cm^{-2} with the fitted lifetimes of 2.37, 3.57, and 4.10 ns for GCHMM, PCHMM, and planar PMMA, respectively. (d) Fitted lifetime as a function of pumping energy densities.

RESULTS AND DISCUSSION

GCHMM Proof-of-Concept. Figure 1a depicts the schematic of a GCHMM. The cross-sectional view of the fabricated free-standing GCHMM is shown in Figure 1b. The detailed fabrication processes of GCHMM and PCHMM are presented in Figures S1 and S2, respectively. Both of the HMM structures are composed of four Au/PMMA bilayers with a thickness of 12/30 nm each, and the corresponding fill fraction of the HMM multilayer is 28.57%. Then, on top of the GCHMM, we added an additional grating nanostructure layer of PMMA containing CdSe/ZnS core-shell QDs; PCHMM (Figure S3) and the reference sample (planar PMMA) did not have any grating nanostructure on its top. Figure S4 shows the high-resolution transmission electron microscopy (HR-TEM) scan of CdSe/ZnS QDs with an average diameter of 6 nm. Figure 1c,d depicts the morphologies of GCHMM under an optical microscope (OM) and atomic force microscope (AFM), respectively. The period, width, and height of the grating nanostructure are 700, 300, and 100 nm, respectively. These grating nanostructures play a role in trapping the emitted photons and an efficient feedback loop of laser action.

The realization of effective dielectric tensor calculation is essential to discover the unique functionalities of GCHMM.

https://doi.org/10.1021/acsami.1c15481
ACS Appl. Mater. Interfaces 2021, 13, 49224−49231

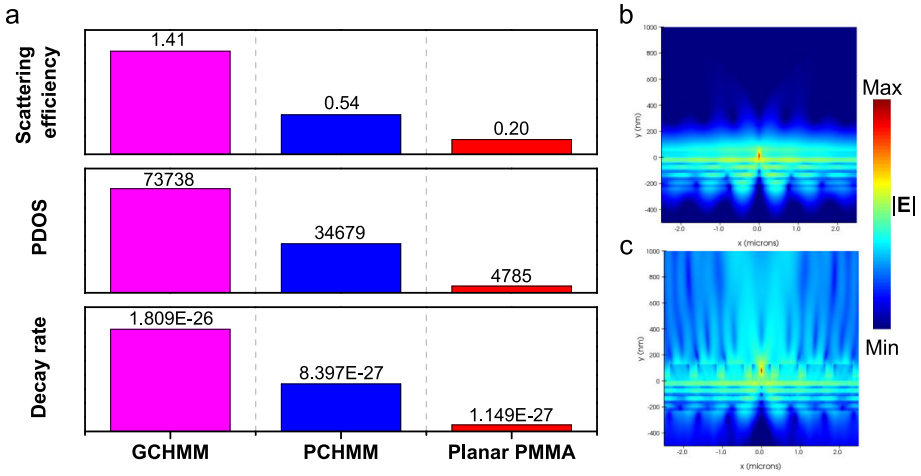

Figure 5. Theoretical simulations. (a) Simulated scattering efficiencies, photonic density of states (PDOS), and decay rates at the emission wavelength center for CdSe/ZnS QDs at 630 nm. Panels (b) and (c) are the cross-sectional views of electric-field distributions for the PCHMM and GCHMM generated by the vertical dipole orientation, respectively. The dipoles are located at the emission center of CdSe/ZnS QDs (marked in the central red area).

According to the effective medium theory, the calculated anisotropic permittivity of the metamaterial shows hyperbolic-type dispersion ($\varepsilon_{\perp} \cdot \varepsilon_{\parallel} < 0$) above a wavelength of 555 nm (Figure S5). Figure 2a shows the iso-frequency curve at 630 nm, the emission central wavelength of CdSe/ZnS QDs. Figure 2b and Figure S6 show the normalized dissipated power spectra with and without losses in Au layers of HMM at a dipole distance of 5 nm away from the HMM surface. We also plotted in Figure S7 the normalized dissipated power spectra of the HMM for an increased dipole−HMM distance of 20 nm. These spectra reveal that the HMM significantly enhances the light-matter interaction of the bottom-layer QDs. Then, the chosen Au/PMMA bilayer with a thickness of 12/30 nm is realized. Also, the HMM structures with four alternative multilayers have been proven to be able to boost the dynamics of charge transfer of semiconductors.[22] The topmost PMMA layer also serves as the capping layer to avoid the quenching effect from the emission of CdSe/ZnS QDs.[19]

Enhanced Random Laser Action. To observe the emission spectra of our device, Figure 3a,b shows the emission spectra of CdSe/ZnS QDs embedded inside the grating nanostructure layer and on top of the planar HMM for the GCHMM and PCHMM on Si substrates, respectively. To explore the random laser action of the emission spectra, we varied the pumping energy density in a range of 0.72−1.39 kW cm^{-2} For the GCHMM, under a pumping energy density of 0.72 kW cm^{-2}, a typical spontaneous emission with a full width at half maximum (FWHM) larger than 10 nm is observed. When the pumping energy densities are above 1.12 kW cm^{-2}, the optical gain overcomes its interior loss. This leads to the appearance of several sharp peaks with an FWHM of less than 1 nm.[37,38] For the same pumping energy densities, below 1.39 kW cm^{-2}, the PCHMM produces broad emission spectra corresponding to spontaneous emissions. All the emission spectra were excited using a pulsed diode laser with a central wavelength of 374 nm focused with an objective lens. The incident laser spot size covers the same volume of CdSe/ZnS QDs for measurements as a fair comparison (Figure S8). In addition, Figure S9a,b shows the emission spectra of CdSe/ZnS QDs embedded inside the PCHMM and placed on top of a Si substrate, respectively. For the PCHMM, with further increase in the pumping energy densities to 2.13 and 2.95 kW cm^{-2}, random lasing peaks are observed, whereas for the CdSe/ZnS QDs on a Si substrate, all the spectra resemble the ones of spontaneous emission for pumping energy densities below 2.95 kW cm^{-2}.

The characterization results of random laser action are shown in Figure 4. The maximum emission intensities are plotted as a function of pumping energy densities (Figure 4a). The fitted lines with relatively flat slopes are spontaneous emissions, and those with relatively sharp slopes are stimulated emissions. The intersections (marked as hollow circles) between the flat and sharp slopes are the lasing thresholds. Figure 4b shows the FWHM of peaks as a function of pumping energy densities retrieved from Figure 4a. The lasing thresholds for the GCHMM and PCHMM are 1.05 and 1.95 kW cm^{-2}, respectively. Importantly, the GCHMM presents 13 times enhancement of extracted emission intensity of laser action, 46% reduced threshold, and 1.8-fold increase in differential quantum efficiency derived from the curve of slopes from the output power to the input pumping power as compared to PCHMM (in Table S1). The temporal coherence length ($L = c/(n\Delta f)$) random laser action is calculated as 265 μm, where c, n, and (Δf) are the velocity of light at vacuum, the refractive index of the medium, and the frequency bandwidth, respectively.[41] This is long enough to form the closed loop paths of the surrounded CdSe/ZnS QDs in PMMA and then achieve the laser action. To consolidate the random laser action, Figure 4c shows the results of lifetime measurements at a pumping energy density of 2.47 kW cm^{-2}, and the lifetimes retrieved from exponential fitting were retrieved for 2.37, 3.57, and 4.10 ns for the GCHMM, PCHMM, and planar PMMA, respectively. The fitted lifetimes as a function of pumping energy density are shown in Figure 4d, and the detailed lifetime measurements under different pumping energy densities are shown in Figure S10. The enhancement of decay rate here is because of the grating nanostructures that GCHMM provides a platform to scatter the light multiple times and stimulate the recombination of electrons and holes. When approaching the lasing threshold, the lifetimes of spontaneous emission in a range from 3.9 to 5.5 ns drop to a range from 2.2 to 3.6 ns of stimulated emission.

https://doi.org/10.1021/acsami.1c15481
ACS Appl. Mater. Interfaces 2021, 13, 49224−49231

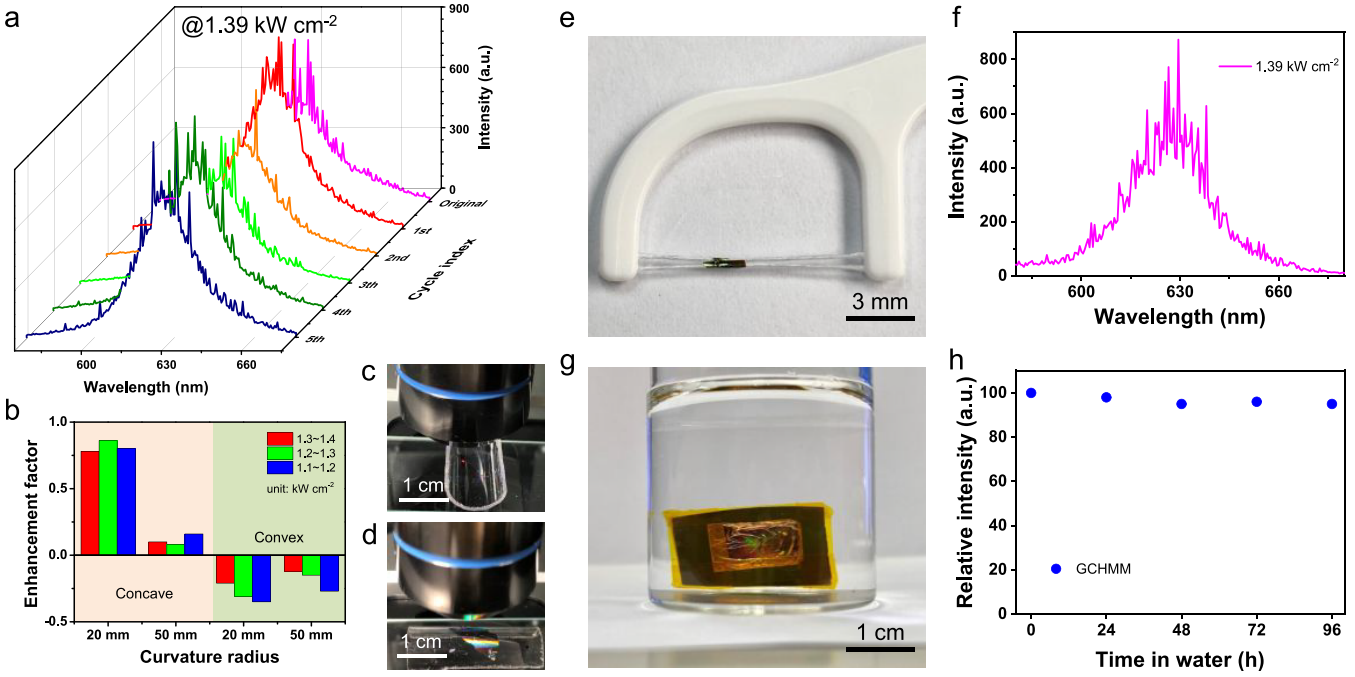

Figure 6. Multi-functions of GCHMM. (a) Emission spectra of laser action with increasing mechanically retransferable cycle indexes up to 5 times under the same pumping energy intensity of 1.39 kW cm^{-2}. (b) Enhancement factors of GCHMM on the concave and convex substrates under the curvature radiuses of 20 and 50 mm as compared to the planar glass substrate. Panels (c) and (d) are the photos of GCHMM on concave and convex glass substrates with a curvature radius of 20 mm, respectively. The red dots are the emission excited under an irradiation of a 374 nm pulsed diode laser at a pumping energy density of 1.39 kW cm^{-2}. (e) GCHMM device attached to the dental floss and forming a smooth surface. (f) emission spectrum of GCHMM attached to the dental floss at a pumping energy density of 1.39 kW cm^{-2}. (g) Photograph of GCHMM in DI water. (h) Relative emission intensity of GCHMM after immersion in DI water.

No laser action is observed for the planar PMMA due to the limited PDOS below a pumping energy intensity of 3.00 kW cm^{-2}, resulting in a relatively higher lifetime. In addition, both the GCHMM and PCHMM samples still support the laser action with the tilted sample holder up to 20° (Figures S11 and S12), which is the additional evidence for the occurrence of random laser action. The trends are similar to the simulated normalized intensity of far-field angular emission as shown in Figure S13.

Theoretical Analysis. To further discover the light−matter interactions, the realization of scattering efficiency, PDOS, and decay rate are essential using a three-dimensional finite-difference time-domain (FDTD) as shown in Figure 5a. The scattering efficiencies for the GCHMM, PCHMM, and planar PMMA are simulated as 1.41, 0.54, and 0.20, respectively, i.e., the GCHMM increases 1.6 times (6.1 times) as compared to the PCHMM (planar PMMA).[42] This is due to the fact that the GCHMM provides an excellent platform to scatter the light for multiple times around the grating nanostructures to boost the random laser action. While considering the radiation from dipole emitters by the approach of a dyadic Green's function,[43] the GCHMM increases 1.1 times (14.4 times) of PDOS and 1.2 times (14.7 times) of the decay rate as compared to the PCHMM (planar PMMA). Figure S14 shows the Purcell factors on top of the PCHMM substrate within 30 nm, demonstrating the optimized design of a multilayer HMM structure at the central emission wavelength for CdSe/ZnS QDs at 630 nm. The Purcell factor is the enhancing ratio of the dipole emitter placed in the structure to that of in the free space. Since the height of the periodical nanostructure is 100 nm, this results in the great enhancement of emission spectra as well as the pronounced decrease in measurements of lifetime.

Light extraction also plays a critical role to greatly enhance the emission intensities of laser action. Owing to the type II dispersion (i.e., $Re(\varepsilon_{\parallel}) < 0$ and $Re(\varepsilon_{\perp}) > 0$) for the proposed HMM structure, the coupling effect leads to side out-coupling.[44] Figure 5b shows the cross-sectional view of electric-field distributions for the PCHMM generated by the vertical dipole orientation at the central emission positions of the QDs/PMMA layer. The energy flow at around the PCHMM is preferable to be guided along the surface and then will be annihilated as a form of evanescent field, limiting the ability to propagate to a far field for the enhancement of light−matter interactions. Importantly, pronounced out-coupling of light extraction can be observed for the GCHMM (Figure 5c). The mechanism of light extraction from the grating nanostructure is that the x component of the k-vector between the interface of HMM and air is continuous, which means that $k_{air,x} = k_{HMM,x}$. However, $k_{HMM,x} > k_{air}$, which implies that $k_{air,z}$ is purely an imaginary number and thus modes become evanescent at the surface. Therefore, grating nanostructures serve as an efficient platform that provides an extra k-vector to translate the evanescent wave into propagating wave and overcome the inherent drawback of side out-coupling for type II dispersion.[44] Remarkably, this benefit makes the GCHMM able to sustain longer coupling duration for 5.7 times and increases the strength of electric-field intensities for 4.0 times compared with the PCHMM (Figure S15). Therefore, the GCHMM with grating structures benefits the trapping of emitted photons and then provides a strong feedback mechanism to trigger the laser action.

https://doi.org/10.1021/acsami.1c15481
ACS Appl. Mater. Interfaces 2021, 13, 49224−49231

Multi-functionalities of GCHMM. Figure 6 shows the novel and multiple functionalities of GCHMM. First, the critical issue of discussing random laser action is to observe the distinct feedback mechanism for the retransferable process of GCHMM as sustainable optoelectronic devices. Figure 6a shows the emission spectra of laser action with an increasing cycle index up to 5 times under the same pumping energy intensity of 1.39 kW cm^{-2}, indicating the stable emissions with a slight fluctuation despite the mechanically retransferable process on different Si substrates. The reason for choosing a pumping energy density of 1.39 kW cm^{-2} for testing the lasing ability of GCHMM is to observe the multi-functions, which cannot be observed for the PCHMM (threshold at 1.95 kW cm^{-2}) and even the planar PMMA (higher threshold) samples. If the chosen pumping energy density is near the threshold, i.e., slight larger than 1.05 kW cm^{-2}, then the emission spectra of laser action could not be pronounced and even hard to distinguish. Therefore, we choose the pumping energy density in between the threshold (1.05 kW cm^{-2}) and 1.95 kW cm^{-2} to emphasize the importance of GCHMM. The GCHMM is covered with a grating nanostructure, which can serve as the protection layer during the retransferable process. Second, the whole GCHMM device is made of a flexible polymer and ductile metal, and hence it is can tolerate large mechanical deformations. To explore the flexibility, Figure 6b shows the enhancement factors of GCHMM on concave and convex substrates under the curvature radiuses of 20 and 50 mm, and the corresponding emission spectra of random laser action are shown in Figure S16. Under a curvature radius of 20 mm, the averaged emission intensity is increased by 81% on a concave substrate (Figure 6c) and decreased by 29% on convex substrate (Figure 6d) as compared to that on the planar glass substrate. Meanwhile, under a curvature radius of 50 mm, the averaged emission intensity is slightly increased by 11% on a concave substrate and decreased by 18% on a convex substrate. These are due to the concave substrate with less curvature radius serving as a more efficient platform to scatter light of multiple reflection processes inside the valley structure.[8,38] Then, the feedback loops are strengthened to boost the random laser action.

Furthermore, the GCHMM device not only shows the adaptability and free-standing properties but also provides sufficient protection to retain excellent stability in deionized (DI) water. We integrate the GCHMM device on a dental floss with the radius of 0.2 mm (Figure 6e), and the surface of GCHMM device seems quite smooth and can even sustain a certain shear stress. The attached GCHMM device also retains stable functionality, and the emission intensity of laser action is very similar to its original condition (Figure 6f), which is quite important and beneficial for the practical integration with optoelectronic devices. In addition, the GCHMM device provides sufficient protection in DI water (Figure 6g) to retain excellent stability for 96 h under a pumping energy intensity of 1.10 kW cm^{-2} (Figure 6h and Figure S17).

The methodology used here, already proven to be used in a flexible meta-device, can be a potential candidate in optoelectronic device applications. These demonstrations of transferrable, adaptable, free-standing, and water-resistant properties are especially important in applications such as guidance of light for fiber-optic communications, where the GCHMM device is attachable to the surface of optical fiber to excite and extract the particular resonance mode out of the fiber. Unlike the conventional metamaterial system and flexible device, the abovementioned characteristic is hardly achievable. In addition, the design of a GCHMM device embedded with different QDs and tunable hyperbolic dispersions can serve as efficient full-color display and white-light illumination in a single segment. Replacing the embedded QDs with upconversion nanoparticles, the GCHMM device is biocompatible and applicable in sensitive night vision goggles and contact lenses. Importantly, the integration of GCHMM device with optoelectronic device applications can be further imaged, such as being attachable on human skin for environmental sensors and real-time monitoring of transferrable healthcare devices. Interestingly, the GCHMM device is embedded inside the freeform sensors for home security and car alarm systems due to the related response of electromagnetic waves. Therefore, the demonstration of GCHMM provides a new paradigm to explore multifunctional features not only for metamaterials but also for flexible optoelectronic devices in future applications.

CONCLUSIONS

In summary, the prototype of GCHMM has been successfully demonstrated by using a convenient and low-cost method. The whole GCHMM device is mechanically foldable, adaptable on freeform surfaces, free-standing, and water-resistant with an ultrathin thickness scaling down to submicron. The GCHMM is composed of four pairs of Au/PMMA multilayers showing hyperbolic-type dispersion, and on top of it is the periodical nanostructure of PMMA with embedded QDs. These QDs serve as the multiple scattering gain media in random laser action. The periodical nanostructure can serve as the efficient platforms to extract light from QDs. Then, the laser action is enhanced 13 times, the threshold is reduced by 46%, and the differential quantum efficiency is increased by 1.8 times as compared to the PCHMM. In addition, as the GCHMM is retransferable on different substrates for several times, it still retains excellent performances as well as shows stable functionality even when transferred to a dental floss with a radius of 0.2 mm. Furthermore, the GCHMM device provides sufficient protection in DI water to retain excellent stability for 96 h. We therefore foresee that the GCHMM will serve as a versatile platform for foldable, adaptable, free-standing, and water-resistant photonic meta-devices in future optoelectronic device applications.

MATERIALS AND METHODS

Fabrication Methods of GCHMM. The detailed fabrication process of GCHMM is presented in Figure S1. The CdSe/ZnS core-shell type QDs are commercially available (Sigma-Aldrich) with the emission wavelength center at 630 nm.

Characterizations of GCHMM. The characterization GCHMM was performed by a dual-beam focused ion beam (FIB)-SEM systems (SEIKO SMI3050SE). The FIB system uses high energy of gallium ions to mill the GCHMM to prepare the sample cross section of the GCHMM. Then, we used the SEM system to examine the composition of multilayers.

Measurement of Laser Action and Lifetime. We used a pulsed diode laser (Picoquant, PDL 800-B) with a central wavelength of 374 nm, a pulsed duration of 70 ps, and a repetition rate of 2.5 MHz to measure the spectra of random laser action and the corresponding lifetime. These spectra and lifetimes were recorded using a Horiba Jobin Yvon TRIAX 320 spectrometer, which is equipped with an OM setup containing a 100× objective lens (Olympus, Japan) with a numerical aperture of 0.9.

https://doi.org/10.1021/acsami.1c15481
ACS Appl. Mater. Interfaces 2021, 13, 49224−49231

Instrumentation of HR-TEM. The HR-TEM image of the CdSe/ZnS QDs was obtained by a TECNAI G2 FEG-TEM operating at 300 kV.

Numerical Simulation. To perform the numerical simulation, we used the commercial electromagnetic software (Lumerical) of an FDTD. The refractive indices of pure PMMA, CdSe/ZnS QDs, and Au were set as 1.49, 1.44, and from the database of Johnson and Christy, respectively.[45,46] We used the perfectly matched layers to cover the boundaries of the computational domain in order to prevent reflection from the domain boundaries. The simulation settings of scattering, PDOS, decay rates, and electric-field distribution are shown in Figure S19–S22.

■ ASSOCIATED CONTENT

Supporting Information

The Supporting Information is available free of charge at https://pubs.acs.org/doi/10.1021/acsami.1c15481.

Fabrication processes of GCHMM and PCHMM, SEM image of PCHMM, HR-TEM of CdSe/ZnS QDs, hyperbolic-dispersion calculations, normalized dissipated power spectra, area of incident laser spot, emission spectra of random laser action, calculations of the performances of GCHMM, lifetime measurements, broad angular emissions, Purcell factors, emission performances using different QDs, time decay of electric-field intensities, emission performances under different curvature radiuses, emission performances after immersion in DI water, and simulation settings (PDF)

■ AUTHOR INFORMATION

Corresponding Author

Yang-Fang Chen − *Department of Physics and Advanced Research Centre for Green Materials Science and Technology, National Taiwan University, Taipei 10617, Taiwan;* orcid.org/0000-0003-1203-5115; Email: yfchen@phys.ntu.edu.tw

Authors

Hung-I Lin − *Department of Physics, National Taiwan University, Taipei 10617, Taiwan;* orcid.org/0000-0001-9849-3138

Hsiang-Yao Tan − *Department of Physics, National Taiwan University, Taipei 10617, Taiwan*

Yu-Ming Liao − *Department of Physics, National Taiwan University, Taipei 10617, Taiwan;* orcid.org/0000-0002-8696-7313

Kun-Ching Shen − *Advanced Remanufacturing and Technology Centre, The Agency for Science, Technology and Research, 637143, Singapore;* orcid.org/0000-0001-7751-7399

Mikhail Y. Shalaginov − *Department of Materials Science and Engineering, Massachusetts Institute of Technology, Cambridge, Massachusetts 02139, United States;* orcid.org/0000-0002-1251-7766

Monika Kataria − *Department of Physics, National Taiwan University, Taipei 10617, Taiwan;* orcid.org/0000-0003-4912-340X

Chih-Ting Chen − *Department of Physics, National Taiwan University, Taipei 10617, Taiwan*

Jun-Wei Chang − *Department of Physics, National Taiwan University, Taipei 10617, Taiwan*

Complete contact information is available at: https://pubs.acs.org/10.1021/acsami.1c15481

Author Contributions

H.I.-L. and H.-Y.T. contributed equally to this work. H.I.-L. and Y.-F.C. conceived the idea of GCHMM. H.-I.L., H.-Y.T., Y.-M.L., and Y.-F.C. discussed the mechanism of random laser action. H.-Y.T. prepared the GCHMM and measured emission spectra. H.-I L. performed simulations. H.-I.L., H.-Y.T., J.-W.C., C.-T.C., K.-C.S., M.Y.S., and Y.-F.C. discussed the mechanism of HMM. H.-I.L. and M.Y.S. calculated the normalized dissipated power spectra. H.-I.L. and M.K. took the TEM image. H.-I.L. and Y.-F.C. wrote the paper. Y.-F.C. supervised the project. All the authors were involved in analyzing the data.

Notes

The authors declare no competing financial interest.

■ ACKNOWLEDGMENTS

This work was financially supported by the "Advanced Research Centre for Green Materials Science and Technology" from The Featured Area Research Centre Program within the framework of the Higher Education Sprout Project by the Ministry of Education (108L9006) and the Ministry of Science and Technology in Taiwan (MOST 108-3017-F-002-002 and MOST 108-2112-M-002-044). Thanks to Ms. Chia-Ying Chien of Ministry of Science and Technology (National Taiwan University) for the assistance in FIB and SEM experiments.

■ REFERENCES

(1) Dian, F. J.; Vahidnia, R.; Rahmati, A. Wearables and the Internet of Things (IoT), Applications, Opportunities, and Challenges: A Survey. *IEEE Access* **2020**, *8*, 69200−69211.

(2) Qaim, W. B.; Ometov, A.; Molinaro, A.; Lener, I.; Campolo, C.; Lohan, E. S.; Nurmi, J. Towards Energy Efficiency in the Internet of Wearable Things: A Systematic Review. *IEEE Access* **2020**, *8*, 175412−175435.

(3) Lai, Y.-C.; Hsiao, Y.-C.; Wu, H.-M.; Wang, Z. L. Waterproof Fabric-Based Multifunctional Triboelectric Nanogenerator for Universally Harvesting Energy from Raindrops, Wind, and Human Motions and as Self-Powered Sensors. *Adv. Sci.* **2019**, *6*, 1801883.

(4) Hua, Q.; Sun, J.; Liu, H.; Bao, R.; Yu, R.; Zhai, J.; Pan, C.; Wang, Z. L. Skin-inspired highly stretchable and conformable matrix networks for multifunctional sensing. *Nat. Commun.* **2018**, *9*, 244.

(5) Wang, C.; Hwang, D.; Yu, Z.; Takei, K.; Park, J.; Chen, T.; Ma, B.; Javey, A. User-interactive electronic skin for instantaneous pressure visualization. *Nat. Mater.* **2013**, *12*, 899−904.

(6) Liu, Y.; Pharr, M.; Salvatore, G. A. Lab-on-Skin: A Review of Flexible and Stretchable Electronics for Wearable Health Monitoring. *ACS Nano* **2017**, *11*, 9614−9635.

(7) Yang, Y.-F.; Hu, H.-W.; Wu, M.-J.; Lin, T.-Y.; Shen, J.-L.; Chen, Y.-F. Stretchable and Broadband Cavity-Free Lasers Based on All 2D Metamaterials. *Adv. Opt. Mater.* **2020**, *8*, 1901326.

(8) Lin, H.-I.; Wang, C.-C.; Shen, K.-C.; Shalaginov, M. Y.; Roy, P. K.; Bera, K. P.; Kataria, M.; Paul Inbaraj, C. R.; Chen, Y.-F. Enhanced laser action from smart fabrics made with rollable hyperbolic metamaterials. *npj Flexible Electronics* **2020**, *4*, 20.

(9) Loke, G.; Yan, W.; Khudiyev, T.; Noel, G.; Fink, Y. Recent Progress and Perspectives of Thermally Drawn Multimaterial Fiber Electronics. *Adv. Mater.* **2020**, *32*, 1904911.

(10) Yan, W.; Dong, C.; Xiang, Y.; Jiang, S.; Leber, A.; Loke, G.; Xu, W.; Hou, C.; Zhou, S.; Chen, M.; Hu, R.; Shum, P. P.; Wei, L.; Jia, X.; Sorin, F.; Tao, X.; Tao, G. Thermally drawn advanced functional fibers: New frontier of flexible electronics. *Mater. Today* **2020**, *35*, 168−194.

(11) Yan, W.; Page, A.; Nguyen-Dang, T.; Qu, Y.; Sordo, F.; Wei, L.; Sorin, F. Advanced Multimaterial Electronic and Optoelectronic Fibers and Textiles. *Adv. Mater.* **2019**, *31*, 1802348.

(12) Zeng, W.; Shu, L.; Li, Q.; Chen, S.; Wang, F.; Tao, X.-M. Fiber-Based Wearable Electronics: A Review of Materials, Fabrication, Devices, and Applications. *Adv. Mater.* **2014**, *26*, 5310−5336.
(13) Poddubny, A.; Iorsh, I.; Belov, P.; Kivshar, Y. Hyperbolic metamaterials. *Nat. Photonics* **2013**, *7*, 948−957.
(14) Cortes, C. L.; Newman, W.; Molesky, S.; Jacob, Z. Quantum nanophotonics using hyperbolic metamaterials. *J. Opt.* **2012**, *14*, No. 063001.
(15) Krishnamoorthy, H. N. S.; Jacob, Z.; Narimanov, E.; Kretzschmar, I.; Menon, V. M. Topological transitions in metamaterials. *Science* **2012**, *336*, 205−209.
(16) Chandrasekar, R.; Wang, Z.; Meng, X.; Azzam, S. I.; Shalaginov, M. Y.; Lagutchev, A.; Kim, Y. L.; Wei, A.; Kildishev, A. V.; Boltasseva, A.; Shalaev, V. M. Lasing Action with Gold Nanorod Hyperbolic Metamaterials. *ACS Photonics* **2017**, *4*, 674−680.
(17) Lin, H.-I.; Yadav, K.; Shen, K.-C.; Haider, G.; Roy, P. K.; Kataria, M.; Chang, T.-J.; Li, Y.-H.; Lin, T.-Y.; Chen, Y.-T.; Chen, Y.-F. Nanoscale Core−Shell Hyperbolic Structures for Ultralow Threshold Laser Action: An Efficient Platform for the Enhancement of Optical Manipulation. *ACS Appl. Mater. Interfaces* **2019**, *11*, 1163−1173.
(18) Wang, P.; Krasavin, A. V.; Viscomi, F. N.; Adawi, A. M.; Bouillard, J.-S. G.; Zhang, L.; Roth, D. J.; Tong, L.; Zayats, A. V. Metaparticles: Dressing Nano-Objects with a Hyperbolic Coating. *Laser Photonics Rev.* **2018**, *12*, 1800179.
(19) Lu, D.; Kan, J. J.; Fullerton, E. E.; Liu, Z. Enhancing spontaneous emission rates of molecules using nanopatterned multilayer hyperbolic metamaterials. *Nat. Nanotechnol.* **2014**, *9*, 48−53.
(20) Shen, K.-C.; Ku, C.-T.; Hsieh, C.; Kuo, H.-C.; Cheng, Y.-J.; Tsai, D. P. Deep-Ultraviolet Hyperbolic Metacavity Laser. *Adv. Mater.* **2018**, *30*, 1706918.
(21) Haider, G.; Lin, H.-I.; Yadav, K.; Shen, K.-C.; Liao, Y.-M.; Hu, H.-W.; Roy, P. K.; Bera, K. P.; Lin, K.-H.; Lee, H.-M.; Chen, Y.-T.; Chen, F.-R.; Chen, Y.-F. A Highly-Efficient Single Segment White Random Laser. *ACS Nano* **2018**, *12*, 11847−11859.
(22) Lee, K. J.; Xiao, Y.; Woo, J. H.; Kim, E.; Kreher, D.; Attias, A.-J.; Mathevet, F.; Ribierre, J.-C.; Wu, J. W.; André, P. Charge-transfer dynamics and nonlocal dielectric permittivity tuned with metamaterial structures as solvent analogues. *Nat. Mater.* **2017**, *16*, 722−729.
(23) Sreekanth, K. V.; Alapan, Y.; ElKabbash, M.; Ilker, E.; Hinczewski, M.; Gurkan, U. A.; De Luca, A.; Strangi, G. Extreme sensitivity biosensing platform based on hyperbolic metamaterials. *Nat. Mater.* **2016**, *15*, 621−627.
(24) Palermo, G.; Lio, G. E.; Esposito, M.; Ricciardi, L.; Manoccio, M.; Tasco, V.; Passaseo, A.; De Luca, A.; Strangi, G. Biomolecular Sensing at the Interface between Chiral Metasurfaces and Hyperbolic Metamaterials. *ACS Appl. Mater. Interfaces* **2020**, *12*, 30181−30188.
(25) Palermo, G.; Sreekanth, K. V.; Maccaferri, N.; Lio, G. E.; Nicoletta, G.; De Angelis, F.; Hinczewski, M.; Strangi, G. Hyperbolic dispersion metasurfaces for molecular biosensing. *NANO* **2020**, *10*, 295−314.
(26) Yang, X.; Yao, J.; Rho, J.; Yin, X.; Zhang, X. Experimental realization of three-dimensional indefinite cavities at the nanoscale with anomalous scaling laws. *Nat. Photonics* **2012**, *6*, 450−454.
(27) Galfsky, T.; Krishnamoorthy, H. N. S.; Newman, W.; Narimanov, E. E.; Jacob, Z.; Menon, V. M. Active hyperbolic metamaterials: enhanced spontaneous emission and light extraction. *Optica* **2015**, *2*, 62.
(28) Lin, H.-I.; Shen, K.-C.; Liao, Y.-M.; Li, Y.-H.; Perumal, P.; Haider, G.; Cheng, B. H.; Liao, W.-C.; Lin, S.-Y.; Lin, W.-J.; Lin, T.-Y.; Chen, Y.-F. Integration of Nanoscale Light Emitters and Hyperbolic Metamaterials: An Efficient Platform for the Enhancement of Random Laser Action. *ACS Photonics* **2018**, *5*, 718−727.
(29) Cao, H.; Zhao, Y. G.; Ho, S. T.; Seelig, E. W.; Wang, Q. H.; Chang, R. P. H. Random Laser Action in Semiconductor Powder. *Phys. Rev. Lett.* **1999**, *82*, 2278−2281.
(30) Wiersma, D. S. The physics and applications of random lasers. *Nat. Phys.* **2008**, *4*, 359−367.
(31) Redding, B.; Choma, M. A.; Cao, H. Speckle-free laser imaging using random laser illumination. *Nat. Photonics* **2012**, *6*, 355.
(32) Wiersma, D. S.; Lagendijk, A. Light diffusion with gain and random lasers. *Phys. Rev. E* **1996**, *54*, 4256−4265.
(33) Chang, S.-W.; Liao, W.-C.; Liao, Y.-M.; Lin, H.-I.; Lin, H.-Y.; Lin, W.-J.; Lin, S.-Y.; Perumal, P.; Haider, G.; Tai, C.-T.; Shen, K.-C.; Chang, C.-H.; Huang, Y.-F.; Lin, T.-Y.; Chen, Y.-F. A White Random Laser. *Sci. Rep.* **2018**, *8*, 2720.
(34) Roy, P. K.; Haider, G.; Lin, H.-I.; Liao, Y.-M.; Lu, C.-H.; Chen, K.-H.; Chen, L.-C.; Shih, W.-H.; Liang, C.-T.; Chen, Y.-F. Multicolor Ultralow-Threshold Random Laser Assisted by Vertical-Graphene Network. *Adv. Opt. Mater.* **2018**, *6*, 1800382.
(35) Shen, T. L.; Hu, H. W.; Lin, W. J.; Liao, Y. M.; Chen, T. P.; Liao, Y. K.; Lin, T. Y.; Chen, Y. F. Coherent Förster resonance energy transfer: A new paradigm for electrically driven quantum dot random lasers. *Sci. Adv.* **2020**, *6*, No. eaba1705.
(36) Liao, Y.-M.; Lai, Y.-C.; Perumal, P.; Liao, W.-C.; Chang, C.-Y.; Liao, C.-S.; Lin, S.-Y.; Chen, Y.-F. Highly stretchable label-like random laser on universal substrates. *Adv. Mater. Technol.* **2016**, *1*, 1600068.
(37) Hsu, Y.-T.; Tai, C.-T.; Wu, H.-M.; Hou, C.-F.; Liao, Y.-M.; Liao, W.-C.; Haider, G.; Hsiao, Y.-C.; Lee, C.-W.; Chang, S.-W.; Chen, Y.-H.; Wu, M.-H.; Chou, R.-J.; Bera, K. P.; Lin, Y.-Y.; Chen, Y.-Z.; Kataria, M.; Lin, S.-Y.; Paul Inbaraj, C. R.; Lin, W.-J.; Lee, W.-Y.; Lin, T.-Y.; Lai, Y.-C.; Chen, Y.-F. Self-Healing Nanophotonics: Robust and Soft Random Lasers. *ACS Nano* **2019**, *13*, 8977−8985.
(38) Hu, H.-W.; Haider, G.; Liao, Y.-M.; Roy, P. K.; Ravindranath, R.; Chang, H.-T.; Lu, C.-H.; Tseng, C.-Y.; Lin, T.-Y.; Shih, W.-H.; Chen, Y.-F. Wrinkled 2D Materials: A Versatile Platform for Low-Threshold Stretchable Random Lasers. *Adv. Mater.* **2017**, *29*, 1703549.
(39) Shi, X.; Liao, Y.-M.; Lin, H.-Y.; Tsao, P.-W.; Wu, M.-J.; Lin, S.-Y.; Hu, H.-H.; Wang, Z.; Lin, T.-Y.; Lai, Y.-C.; Chen, Y.-F. Dissolvable and Recyclable Random Lasers. *ACS Nano* **2017**, *11*, 7600−7607.
(40) Walpole, J. N.; Kintzer, E. S.; Chinn, S. R.; Wang, C. A.; Missaggia, L. J. High-power strained-layer InGaAs/AlGaAs tapered traveling wave amplifier. *Appl. Phys. Lett.* **1992**, *61*, 740−742.
(41) Akcay, C.; Parrein, P.; Rolland, J. P. Estimation of longitudinal resolution in optical coherence imaging. *Appl. Opt.* **2002**, *41*, 5256−5262.
(42) Bohren, C. F.; Huffman, D. R. Absorption and Scattering by an Arbitrary Particle. In *Absorption and Scattering of Light by Small Particles*, 2 ed.; Wiley-VCH Verlag GmbH: 2007; pp. 57−81.
(43) Novotny, L.; Hecht, B. *Principles of Nano-Optics.* Cambridge Univ. Press: Cambridge 2006; pp. 13−44.
(44) Ferrari, L.; Smalley, J. S. T.; Fainman, Y.; Liu, Z. Hyperbolic metamaterials for dispersion-assisted directional light emission. *Nanoscale* **2017**, *9*, 9034−9048.
(45) Pillonnet, A.; Fleury, P.; Chizhik, A. I.; Chizhik, A. M.; Amans, D.; Ledoux, G.; Kulzer, F.; Meixner, A. J.; Dujardin, C. Local refractive index probed via the fluorescence decay of semiconductor quantum dots. *Opt. Express* **2012**, *20*, 3200−3208.
(46) Johnson, P. B.; Christy, R. W. Optical Constants of the Noble Metals. *Phys. Rev. B* **1972**, *6*, 4370−4379.

https://doi.org/10.1021/acsami.1c15481
ACS Appl. Mater. Interfaces 2021, 13, 49224−49231